Biomimetic Mineralization

DOI: 10.1002/anie.201301184

Heterostructured Calcium Carbonate Microspheres with Calcite Equatorial Loops and Vaterite Spherical Cores**

Sha-Sha Wang, Andreas Picker, Helmut Cölfen, and An-Wu Xu**

Biominerals are highly organized composites of inorganic and organic materials created by living organisms; they include oyster shells, coral, ivory, sea urchin spines, magnetic crystals in magnetotactic bacteria, and human bones. Intriguing examples of biominerals are frequently considered as inspirations for materials science because of their superior materials properties, environmentally friendly synthesis, and complex shapes with hierarchical structures. In biomineralization, the organization of matter into highly ordered superstructures is observed. Simultaneous control over the shape, sizes, and phase of inorganic materials from the nanometer up to the macroscopic scale is an important characteristic of biomineralization.[1]

In some cases, delicate structures cannot be fabricated by a simple atom-by-atom amplification process; instead, they are developed through more complicated mesoscale transformations.[2] In these processes, nanocrystals are formed and then self-assemble in a controlled way because their surfaces contain face-specific information. In the simplest case, this can be attributed to the different surface energies of the crystal facets.[3]

In order to get well-defined crystals with unique structures in the nanometer and micrometer range, it is crucial to control the crystallization processes.[4] This mesoscopic assembly can be achieved by the use of many different additives, such as double hydrophilic block copolymers (DHBCs),[5] biopolymers,[6] synthetic macromolecules,[7] low-molar-mass additives,[8] and self-assembled monolayers.[9] Previous studies mainly focused on the use of a single additive for crystallization control, whereas a combination of two different functional additives in crystallization processes controlled by distinct additive distribution and functions at different reaction stages has been rarely investigated.[10]

[*] S. S. Wang, Prof. Dr. A. W. Xu
Division of Nanomaterials and Chemistry
Hefei National Laboratory for Physical Sciences at Microscale
University of Science and Technology of China
Hefei 230026 (China)
E-mail: anwuxu@ustc.edu.cn
A. Picker, Prof. Dr. H. Cölfen
Physical Chemistry, University of Konstanz
Universitätsstrasse 10
Box 714, 78457 Konstanz (Germany)
E-mail: helmut.coelfen@uni-konstanz.de

[**] We acknowledge support from the National Basic Research Program of China (2010CB934700, 2011CB933700) and the National Natural Science Foundation of China (21271165).

Supporting information for this article is available on the WWW under http://dx.doi.org/10.1002/anie.201301184.

Heterostructured biominerals exhibiting domains consisting of two (or more) different polymorphs are omnipresent in Nature. The otoliths of piranhas, for instance, contain three polymorphs of calcium carbonate (calcite, vaterite, and aragonite).[11] Mussel shells consist of an outer prismatic calcite layer and an inner aragonite tablet layer. However, the coexistence of more than one $CaCO_3$ polymorph in the same particle is rarely observed in biomineralization as well as in in vitro studies of crystallization. Here, we present remarkably shaped $CaCO_3$ crystals which were grown in the presence of poly(sodium 4-styrenesulfonate) (PSS) and folic acid (FA; see Figure S1 in the Supporting Information) by a nonclassical particle-mediated crystallization pathway. We provide the first example of spherical vaterite cores, surrounded by equatorial loops consisting of three-dimensionally arranged calcite nanobricks. High-resolution transmission electron microscopy (HRTEM) and selected-area electron diffraction (SAED) results indicate that the equatorial calcite loops arise from the in situ transformation of vaterite intermediates. A mechanism involving temporary amorphous calcium carbonate (ACC) precursors and delayed gradual phase transformations is proposed and discussed in detail. Our findings will thus contribute to the general understanding of the crystallization of heterostructured biomimetic materials as a consequence of the combination of kinetics and thermodynamics.

The heterostructured calcium carbonate microspheres with equatorial loops were obtained by a simple gas-diffusion method[12] in the presence of PSS and FA (see the Experimental Section in the Supporting Information). PSS is a polymer with a high density of negatively charged sulfonate groups and was already proven to modify the crystallization of inorganic minerals in several previous studies of bio-inspired mineralization.[13] FA (also called vitamin B_9) is indispensable for many body functions such as the promotion of cell division and growth, and the stabilization of DNA.[14] FA is insoluble in acidic aqueous solution, whereas in alkaline solution it becomes soluble and forms anions. The morphology and composition of the obtained crystals (PSS 1 g L^{-1}, FA 0.5 g L^{-1}, and $[CaCl_2] = 10$ mM after 2 days of crystallization) were examined by scanning electron microscopy (SEM; Figure 1). The sample consists almost entirely of uniform microspheres with equatorial loops (Figure 1a). The typical diameters of the spheres are in the range of 8–18 μm, the width of an equatorial loop ranges from 0.6 to 2.5 μm. Closer examination of a single sphere (Figure 1b) reveals that each equatorial loop consists of oriented bricklike crystals with regular faces and sharp edges. In recent studies nanoparticles were suggested as building units of biominerals in combination with a brick-by-brick formation mechanism; several

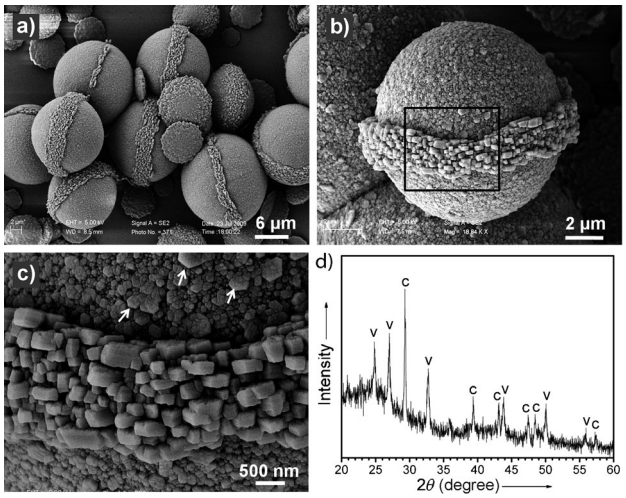

Figure 1. SEM images (a–c) and XRD pattern (d) of the heterostructured calcium carbonate microspheres with an equatorial loop grown for 2 days. [PSS] = 1 g L^{-1}, [FA] = 0.5 g L^{-1}, [$CaCl_2$] = 10 mM. The high-resolution SEM image (c) is taken from the marked region in (b). White arrows indicate pronounced vaterite hexagonal crystals. In (d) the diffraction peaks from calcite are labeled "c" (JCPDS card no. 47-1743); "v" indicates vaterite (JCPDS card no. 33-0268).

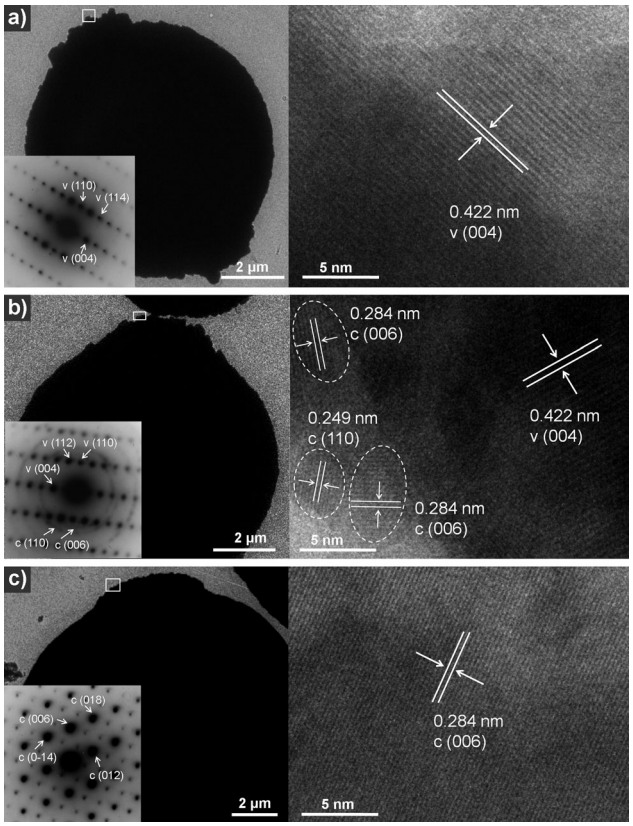

Figure 2. Time-resolved TEM analysis of the calcium carbonate loops after a) 1 d, b) 1.5 d, and c) 2 d. HRTEM images recorded for the equatorial loops (indicated by white boxes) show clearly resolved lattices. Insets show the corresponding SAED patterns: a) vaterite, b) coexisting vaterite and calcite, and c) calcite. [PSS] = 1 g L^{-1}, [FA] = 0.5 g L^{-1}, [$CaCl_2$] = 10 mM. Labels "c" and "v" denote calcite and vaterite, respectively.

biominerals exhibit uniform crystallographic orientation of the nanocrystals and are thus mesocrystals.[15] In the structures in Figure 1, the bricklike crystals in the equatorial loop are arranged perpendicular to the surface of the sphere, while the hexagonal platelet crystals in the core grow along the tangential direction of the spherical surface. In the high-resolution SEM image (Figure 1 c) the nanobuilding blocks on the surface of the sphere exhibit a hexagonal shape (marked with arrows), which is characteristic for vaterite.[16] In contrast, the equatorial loop is composed of rhombohedral building units which are much bigger than the hexagonal particles on the core surface. In view of this unexpected structure with distinct segments, central questions concerning the composition and crystalline phases of the superstructures arise. X-ray diffraction (XRD) analysis (Figure 1 d) indicates a mixture of two crystal phases (calcite and vaterite) in the sample after 2 d of growth. We examined many SEM images and did not observe other calcite sources. Based on these results, we assume that these kinetically captured calcium carbonate crystals are spherical heterostructures with spherical vaterite cores and equatorial calcite loops (denoted as vaterite@calcite).

HRTEM and SAED measurements of the sample after 2 d of growth confirm the vaterite-based phase of the microsphere cores (Figure S2). However, further questions arise regarding the crystal phase of the equatorial loops. There is a transition of microstructures and polymorphs of the equatorial loops with increasing growth time. Figure 2 a shows a typical TEM image of the calcium carbonate microspheres with an equatorial loop after 1 d of crystallization. The corresponding HRTEM image recorded for the loop shows resolved lattice fringes of vaterite (004) planes (d = 0.422 nm), which is further confirmed by SAED (inset in Figure 2 a). An apparent transformation of vaterite into calcite in the edge of the equatorial loop occurs in the 1.5 d sample, as shown in Figure 2 b. The clear observations of multiple randomly oriented domains with clear lattice fringes indicate the emergence of newly formed crystalline areas embedded within the original vaterite framework; the lattice spacings are determined to be 0.249 and 0.284 nm, which is in good agreement with the (110) and (006) crystal planes of calcite, respectively. The corresponding SAED pattern (inset in Figure 2 b) can be indexed with both hexagonal vaterite and randomly distributed calcite crystalline phases. This indicates the coexistence of calcite and vaterite nanocrystals in one ensemble of each sphere. The calcite crystalline domains originate from partial vaterite-to-calcite transformation, and provide nucleation sites for further phase transformation to the more stable calcite phase. These calcite crystalline domains undergo continuous reorganization until they find a perfect lattice match and fuse to a highly oriented calcite mesocrystalline loop in the 2 d sample, where no vaterite phase in the equatorial loop can be detected (Figure 2 c). The appearance of periodic diffraction spots and the well-resolved lattice fringes of calcite (006) planes indicate that these originally randomly nucleated particles have aligned and fused into highly oriented aggregates and diffract now as a single crystal. These results demonstrate that

equatorial calcite loops evolve from the original vaterite phase. Although the underlying mechanisms for the formation of a new calcite phase have not yet been unraveled, it is clear that randomly distributed active sites in the edge of the equatorial loop serve as nucleation sites for the in situ evolution of a new stable calcite phase.

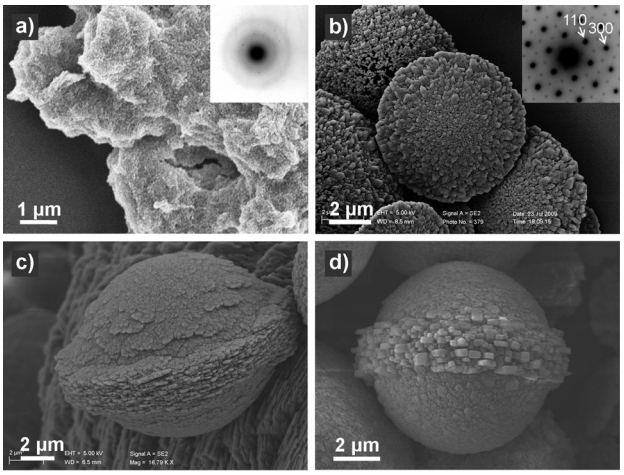

Figure 3. SEM images of the time-resolved experiments: a) 5 h, b) 16 h, c) 1 d, and d) 2 d. [PSS] = 1 g L^{-1}, [FA] = 0.5 g L^{-1}, [$CaCl_2$] = 10 mM. Insets are the corresponding SAED patterns: a) amorphous, b) vaterite.

SEM results of time-resolved experiments (Figure 3) give a clear record of the changes in both the crystal shape and the modification of the heterostructured vaterite microspheres with calcite equators. At a very early stage, probably a few hours after the reaction had started, amorphous calcium carbonate (ACC) nanoparticles with irregular morphologies were formed. Figure 3a shows the corresponding SEM and SAED measurements after a reaction time of 5 h. The formation and transformation of amorphous precursor nanoparticles is very often the first step in nonclassical crystallization pathways.[17] These ACC nanoparticles crystallized and aggregated to produce vaterite platelets after growth for 16 h (Figure 3b). Each platelet can be described as an agglomeration of nanoparticles that share the same three-dimensional orientation; this is in agreement with the reported alignment of vaterite nanoplatelets by oriented attachment in a gas-diffusion crystallization of calcium carbonate.[18] Upon further attachment of nanoparticles, predominantly on the upper and lower surfaces of the intermediate vaterite plate, the $CaCO_3$ platelets grow thicker along the *c*-axis direction of the plates to form discoid particles while the equatorial loop begins to develop simultaneously in the 1 d sample (Figure 3c). After 2 days of growth, calcium carbonate microspheres with bricklike superstructures on the equator have finally formed (Figure 3d). The growth route revealed by time-resolved experiments demonstrates that heterostructured calcium carbonate spheres develop from intermediate vaterite platelets, while the former plate edges transform into the equatorial calcite loop. Additionally, SEM images of a broken $CaCO_3$ sphere (Figures S3 and S5b) clearly show that the calcite equator is arranged around the spherical shell rather than passing across the body of the sphere, indicating that the calcite band forms a ring but not a disk.

To further validate this proposed growth route, we provide more evidence. While most calcium carbonate microspheres exhibit only one equatorial loop, intersecting loops can be occasionally observed. SEM images of time-resolved experiments for such a remarkable $CaCO_3$ microsphere are shown in Figure S4, which clearly indicate the evolution of a sphere with two intersecting brick-wall equators. After a reaction time of 16 h, two intersecting platelets appear in this scenario (Figure S4a). After 1 d reaction, both of the crossed platelets grow thicker (Figure S4b). A remarkable $CaCO_3$ sphere with two intersecting brick-wall equators is observed after 2 d growth (Figure S4c). This shape evolution process further supports our proposed transition mechanism: superstructured vaterite spheres evolve from the intermediate platelets, while the platelet edges finally transform into the brick-wall calcite equators.

Upon prolonged crystallization time, metastable vaterite subsequently transforms into calcite (Ostwald's rule of stages), as shown in Figure S5. The initial transformation is proposed to take place in the equatorial loop at the expense of the vaterite particles. This transformation process is remarkably slower than the previously reported vaterite-to-calcite transition which took place within 7 h.[19] In our case, the spherical core dissolves gradually while the calcite brick-wall equator remains intact. Later, calcite crystals in the loops grow bigger and bigger at the cost of the sacrificed vaterite spheres, thus leaving behind dimples on the surface of rhombohedral calcite. This polymorphic phase transformation behavior is similar to the growth of the previously reported hollow spheres made up of calcite rhombohedra in the presence of poly(ethylene oxide)-*block*-poly(methacrylic acid).[20] After growth for 7 days, only large calcite crystals can be observed.

Nucleation and crystal growth will unavoidably result in the incorporation of additive molecules into the three-dimensional crystals, forming organic–inorganic hybrid structures. Thermogravimetric analysis (TGA) indicates that 2.8 wt% PSS and 2.4 wt% FA were occluded into the crystals (Figure S6). FA itself has bright yellow color (Figure S7a), while PSS and $CaCO_3$ are white powders. As-synthesized heterostructured $CaCO_3$ microspheres exhibit a pale yellow color (Figure S7b), implying the presence of abundant FA molecules in the crystals. In addition to the inclusion of FA molecules into vaterite, the adsorption of FA onto calcite can also be observed (Figure S8).

The additive molecules likely play an important role in inhibiting and tuning the crystallization of inorganic species, leading to the formation of different crystal polymorphs. The multiple effects of additives can be quantitatively classified according to their possible interactions with $CaCO_3$ prenucleation species by titration experiments (see the Experimental Section in the Supporting Information).[21] Typical curves (Figure 4) describe the development of the free ion product with time and the amount of calcium ions added. Titrations

were performed for a reference case (only carbonate buffer) and three additive cases (PSS, FA, and PSS/FA). Compared to the reference experiment, the curve in the presence of FA shows a lower slope indicating the binding of more calcium ions to carbonate ions and thus more stabilized prenucleation clusters. The linear onset of the calcium development indicates that there is no binding affinity between calcium ions and FA molecules. However, strong calcium binding is observed in experiments with PSS and with the PSS/FA mixture. The corresponding calcium binding capacities of PSS and FA were determined in independent titration experiments. While FA molecules do not show any calcium binding, approximately 0.21 Ca^{2+} ions are bound per PSS monomer at pH 9. In Figure 4, the solid straight line and dashed straight line have the same *x*-axis intercept, indicating that also in the

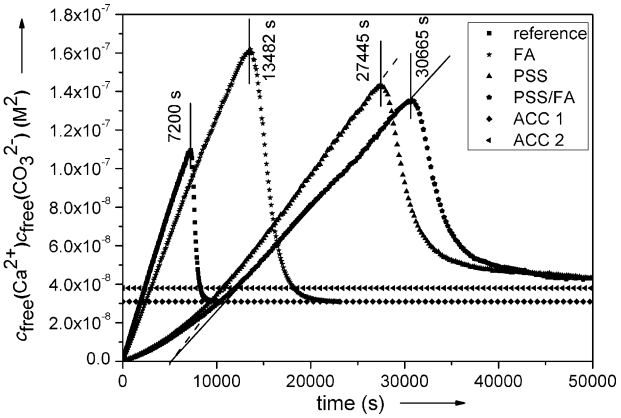

Figure 4. Time development of free ion product measured in 10 mM carbonate buffer solution without (reference) and with additives (FA (1 g L^{-1}) only, PSS (2 g L^{-1}) only, and PSS (2 g L^{-1})/FA (1 g L^{-1}) mixture) at constant pH 9. Two different solubility products of ACC phases of roughly 3.1×10^{-8} M^2 (ACC 1) and 3.8×10^{-8} M^2 (ACC 2) are related to the amorphous phases exhibiting calcitic short-range order and vateritic short-range order, respectively.

FA/PSS combination the binding capacity for calcium ions can be entirely attributed to PSS. A second feature of the titration curves in the presence of additives is that nucleation point is retarded compared to that of the reference, indicated by the peak maximum. The inhibition of nucleation demonstrates that the addition of either FA or PSS stabilizes prenucleation clusters against aggregation which would subsequently lead to nucleation. After nucleation, the ion product drops and reaches solubility products of the precipitated phases. In the case of PSS and the PSS/FA mixture, the reached solubility product corresponds to the amorphous phase exhibiting vateritic short-range order, while the reference and FA curve reach the solubility of the calcitic ACC phase.[22]

Based on these experiments, we conclude that PSS can stabilize the vaterite phase (Figure S9) while FA alone cannot (Figure S8). Regarding the kinetic capture of biphasic heterostructures, further information could be obtained from fluorescence microscopy measurements. Because of the fluorescence characteristic of FA molecules and nonfluorescent PSS, photoluminescence (PL) properties of $CaCO_3$ microspheres could display the distribution of occluded FA within the $CaCO_3$ crystals during crystallization.[23] As shown in Figure S10, upon excitation by ultraviolet light with a wavelength of 370 nm, the whole body of $CaCO_3$ microspheres radiates blue light: It can be clearly seen that the equatorial loop is more pronounced than the core, indicating that it contains more FA molecules than the sphere body. This is due to a fact that at the low initial pH value of 4, FA molecules are insoluble while PSS can dissolve in water. The sulfonate groups are bound Ca^{2+} ions, so that the primary clusters of calcium carbonate and subsequently formed vaterite platelets occlude a lot of PSS. Moreover, a decreasing concentration gradient of the occluded PSS exists within each platelet from the inside to the outside.[24] As the reaction proceeds, the pH increases, to a final value of 9. Since FA is deprotonated and soluble in water the electrostatic repulsion between FA and PSS results in the incorporation of less PSS but more FA in the loops. Control experiments demonstrate that PSS can temporarily stabilize the vaterite phase but FA cannot (Figure S8 and S9). Therefore, the loop regions with high FA content are assumed to generate nucleation sites for vaterite-to-calcite phase transformation, as FA can not inhibit the formation of calcite (Figure S8). On the other hand, the vaterite phase in the sphere body can be temporarily stabilized by PSS (Figure S9). The distinct distribution of the two additives resulting in different crystalline phases is proposed to be the origin of the formation of the unexpected heterostructured vaterite@calcite microspheres. To prove this assumption, we performed control experiments by addition of FA after the crystalllization had started (see Figure S11). Vaterite spheres are observed only in the presence of PSS for 1 d reaction (Figure S11 a), which are similar to those shown in Figure 3 c, indicating the dominant role PSS plays in the formation of vaterite spheres at the early stage. After 1 d reaction, FA was added into the above solution to explore what would happen. With further crystallization for another 1 d after addition of FA, newly formed calcite shells encapsulate the initial vaterite spheres, as shown in Figure S11 b,d. It is obvious that obtained heterostructured $CaCO_3$ spheres have vaterite cores and calcite shells (indicated by arrows in Figure S11 d), illustrating that FA indeed induces the growth of the calcite shell at the later stage of crystallization. FA was added to the solution of vaterite spheres, and FA molecules were uniformly distributed on the whole surface of vaterite spheres; therefore, calcite shells instead of calcite loops were formed on vaterite. Additionally, Figure S11c reveals that in the absence of FA, similar vaterite spheres with equatorial loops are produced in the presence of PSS for 2 d growth. However, these equatorial loops exhibit a characteristic morphology of vaterite platelets instead of calcite bricks. The results of control experiments provide strong support for the fact that the inclusion of FA in the equatorial loops is the key factor for the generation of the calcite loops.

Taken together, the synergistic effect of FA and PSS—individually stabilizing and inducing different calcium carbonate phases at different reaction stages—leads to the formation of the complex vaterite@calcite heterostructures

for the first time. Two $CaCO_3$ polymorphs could be obtained and stabilized in one and the same particle for several days, while the previously reported vaterite-to-calcite transformation usually takes place at the same reaction stages. This is a typical model system for the basic investigation of the combination of kinetics and thermodynamics in crystallization processes. The $CaCO_3$ microspheres formed by a nonclassical particle-mediated process also indicate the importance of mesoscopic transformations in coexisting polymorph crystallization. The controlled distribution of various growth modifiers with distinct functions in crystals should open up new possibilities for rational design in crystal morphogenesis, polymorphs, and hierarchical superstructures.

Received: February 9, 2013
Published online: April 29, 2013

Keywords: bio-inspired mineralization · calcium carbonate · coexisting polymorphs · crystallization processes · heterostructures

[1] a) H. A. Lowenstam, S. Weiner, *On Biomineralization*, Oxford University Press, New York, **1989**; b) E. Bäuerlein, *Biomineralization*, Wiley-VCH, Weinheim, **2000**; c) S. Mann, *Biomineralization, Principles and Concepts in Bioinorganic Materials Chemistry*, Oxford University Press, Oxford, **2001**; d) S. Mann, J. Webb, R. J. P. Williams, *Biomineralization*, VCH, Weinheim, **1989**; e) M. Antonietti, G. A. Ozin, *Chem. Eur. J.* **2004**, *10*, 28; f) S. Weiner, I. Sagi, L. Addadi, *Science* **2005**, *309*, 1027.

[2] a) H. Cölfen, S. Mann, *Angew. Chem.* **2003**, *115*, 2452; *Angew. Chem. Int. Ed.* **2003**, *42*, 2350; b) H. Cölfen, M. Antonietti, *Angew. Chem.* **2005**, *117*, 5714; *Angew. Chem. Int. Ed.* **2005**, *44*, 5576; c) A. W. Xu, M. Antonietti, S. H. Yu, H. Cölfen, *Adv. Mater.* **2008**, *20*, 1333.

[3] A. W. Xu, Y. R. Ma, H. Cölfen, *J. Mater. Chem.* **2007**, *17*, 415.

[4] a) F. C. Meldrum, H. Cölfen, *Chem. Rev.* **2008**, *108*, 4332; b) Y. Peng, A. W. Xu, B. Deng, M. Antonietti, H. Cölfen, *J. Phys. Chem. B* **2006**, *110*, 2988.

[5] a) H. Cölfen, *Macromol. Rapid Commun.* **2001**, *22*, 219; b) H. T. Shi, L. M. Qi, J. M. Ma, H. M. Cheng, *J. Am. Chem. Soc.* **2003**, *125*, 3450; c) T. X. Wang, A. W. Xu, H. Cölfen, *Angew. Chem.* **2006**, *118*, 4561; *Angew. Chem. Int. Ed.* **2006**, *45*, 4451; d) H. Cölfen, M. Antonietti, *Langmuir* **1998**, *14*, 582.

[6] a) E. G. Bellomo, T. J. Deming, *J. Am. Chem. Soc.* **2006**, *128*, 2276; b) Y. Yao, W. Y. Dong, S. M. Zhu, X. H. Yu, D. Y. Yan, *Langmuir* **2009**, *25*, 13238.

[7] J. D. Hartgerink, E. Beniash, S. I. Stupp, *Science* **2001**, *294*, 1684.

[8] a) C. A. Orme, A. Noy, A. Wierzbicki, M. T. McBride, M. Grantham, H. H. Teng, P. M. Dove, J. J. DeYoreo, *Nature* **2001**, *411*, 775; b) L. A. Estroff, C. D. Incarvito, A. D. Hamilton, *J. Am. Chem. Soc.* **2004**, *126*, 2; c) A. W. Xu, Q. Yu, W. F. Dong, M. Antonietti, H. Cölfen, *Adv. Mater.* **2005**, *17*, 2217.

[9] a) J. Aizenberg, A. J. Black, G. M. Whitesides, *Nature* **1999**, *398*, 495; b) B. R. Heywood, S. Mann, *Adv. Mater.* **1994**, *6*, 9; c) Y.-J. Han, L. M. Wysocki, M. S. Thanawala, T. Siegrist, J. Aizenberg, *Angew. Chem.* **2005**, *117*, 2438; *Angew. Chem. Int. Ed.* **2005**, *44*, 2386; d) H. Li, L. A. Estroff, *J. Am. Chem. Soc.* **2007**, *129*, 5480.

[10] a) M. Li, H. Cölfen, S. Mann, *J. Mater. Chem.* **2004**, *14*, 2269; b) L. M. Qi, J. Li, J. M. Ma, *Adv. Mater.* **2002**, *14*, 300.

[11] A. M. Oliveira, M. Farina, *Naturwissenschaften* **1996**, *83*, 133.

[12] J. Ihli, P. Bots, A. Kulak, L. G. Benning, F. C. Meldrum, *Adv. Funct. Mater.* **2013**, DOI: 10.1002/adfm.201201742.

[13] a) T. X. Wang, H. Cölfen, M. Antonietti, *J. Am. Chem. Soc.* **2005**, *127*, 3246; b) A. H. Cai, X. R. Xu, H. Pan, J. H. Tao, R. Liu, R. K. Tang, K. Cho, *J. Phys. Chem. C* **2008**, *112*, 11324; c) Z. Liu, X. D. Wen, X. L. Wu, Y. J. Gao, H. T. Chen, J. Zhu, P. K. Chu, *J. Am. Chem. Soc.* **2009**, *131*, 9405; d) A. S. Schenk, I. Zlotnikov, B. Pokroy, N. Gierlinger, A. Masic, P. Zaslansky, A. N. Fitch, O. Paris, T. H. Metzger, H. Cölfen, P. Fratzl, B. Aichmayer, *Adv. Funct. Mater.* **2012**, *22*, 4668.

[14] a) M. J. Boot, R. P. M. Steegers-Theunissen, R. E. Poelmann, L. V. Iperen, J. Lindemans, A. C. G.-D. Groot, *Dev. Dyn.* **2003**, *227*, 301; b) M. Fenech, *Mutat. Res.* **2001**, *475*, 57.

[15] a) Y. Oaki, A. Kotachi, T. Miura, H. Imai, *Adv. Funct. Mater.* **2006**, *16*, 1633; b) J. Seto, Y. R. Ma, S. A. Davis, F. Meldrum, A. Gourrier, Y.-Y. Kim, U. Schilde, M. Sztucki, M. Burghammer, S. Maltsev, C. Jäger, H. Cölfen, *Proc. Natl. Acad. Sci. USA* **2012**, *109*, 3699.

[16] A. W. Xu, M. Antonietti, H. Cölfen, Y. P. Fang, *Adv. Funct. Mater.* **2006**, *16*, 903.

[17] H. Cölfen, *Mesocrystals and Nonclassical Crystallization*, Wiley, Chichester **2008**.

[18] N. Gehrke, H. Cölfen, N. Pinna, M. Antonietti, N. Nassif, *Cryst. Growth Des.* **2005**, *5*, 1317.

[19] A. Richter, D. Petzold, H. Hofmann, B. Ullrich, *Chem. Tech.* **1996**, *48*, 271.

[20] S. H. Yu, H. Cölfen, M. Antonietti, *J. Phys. Chem. B* **2003**, *107*, 7396.

[21] a) D. Gebauer, A. Völkel, H. Cölfen, *Science* **2008**, *322*, 1819; b) D. Gebauer, H. Cölfen, A. Verch, M. Antonietti, *Adv. Mater.* **2009**, *21*, 435.

[22] D. Gebauer, P. N. Gunawidjaja, J. Y. P. Ko, Z. Bacsik, B. Aziz, L. J. Liu, Y. F. Hu, L. Bergström, C.-W. Tai, T.-K. Sham, M. Edén, N. Hedin, *Angew. Chem.* **2010**, *122*, 9073; *Angew. Chem. Int. Ed.* **2010**, *49*, 8889.

[23] N. Gartmann, D. Brühwiler, *Angew. Chem.* **2009**, *121*, 6472; *Angew. Chem. Int. Ed.* **2009**, *48*, 6354.

[24] Y. X. Gao, S. H. Yu, H. P. Cong, J. Jiang, A. W. Xu, W. F. Dong, H. Cölfen, *J. Phys. Chem. B* **2006**, *110*, 6432.

